Probing the slope of cluster mass profile with gravitational Einstein rings: application to Abell 1689

H. Tu, Marceau Limousin, B. Fort, C. G. Shu, J. F. Sygnet, E. Jullo, J. P. Kneib, Johan Richard

Mon. Not. R. Astron. Soc. **386,** 1169–1178 (2008) doi:10.1111/j.1365-2966.2008.12929.x

Probing the slope of cluster mass profile with gravitational Einstein rings: application to Abell 1689

H. Tu,[1,2,3★] M. Limousin,[4] B. Fort,[2] C. G. Shu,[1,3] J. F. Sygnet,[2] E. Jullo,[5,6] J. P. Kneib[6,7] and J. Richard[7]

[1]*Department of Physics, Shanghai Normal University, 100 Guilin Road, Shanghai 200234, China*
[2]*Institut d'Astrophysique de Paris, 98bis Bvd Arago, 75014 Paris, France*
[3]*Shanghai Astronomical Observatory, 80 Nandan Road, Shanghai 200030, China*
[4]*Dark Cosmology Centre, Niels Bohr Institute, University of Copenhagen, Juliane Maries Vej 30, 2100 Copenhagen, Denmark*
[5]*European Southern Observatory, Alonso de Cordova, Santiago, Chile*
[6]*OAMP, Laboratoire d'Astrophysique de Marseille – UMR 6110 – Traverse du siphon, 13012 Marseille, France*
[7]*Department of Astronomy, California Institute of Technology, 105-24, Pasadena, CA 91125, USA*

Accepted 2008 January 6. Received 2008 January 4; in original form 2007 October 10

ABSTRACT

The strong lensing modelling of gravitational 'rings' formed around massive galaxies is sensitive to the amplitude of the external shear and convergence produced by nearby mass condensations. In current wide-field surveys, it is now possible to find out a large number of rings, typically 10 gravitational rings per square degree. We propose here, to systematically study gravitational rings around galaxy clusters to probe the cluster mass profile beyond the cluster strong lensing regions. For cluster of galaxies with multiple arc systems, we show that rings found at various distances from the cluster centre can improve the modelling by constraining the slope of the cluster mass profile. We outline the principle of the method with simple numerical simulations and we apply it to three rings discovered recently in Abell 1689. In particular, the lens modelling of the three rings confirms that the cluster is bimodal, and favours a slope of the mass profile steeper than isothermal at a cluster radius $\sim$300 kpc. These results are compared with previous lens modelling of Abell 1689 including weak lensing analysis. Because of the difficulty arising from the complex mass distribution in Abell 1689, we argue that the ring method will be better implemented on simpler and relaxed clusters.

Key words: gravitational lensing – galaxies: clusters: general – dark matter.

1 INTRODUCTION

In recent years, the modelling of cluster mass distribution has been progressively improved by (i) coupling the strong lensing (SL) analysis in cluster cores with weak lensing (WL) measurements at large radius (e.g. Gavazzi 2005; Cacciato et al. 2006; Limousin et al. 2007b); (ii) SZ measurements (e.g. Doré et al. 2001; Zaroubi et al. 2001; Sereno 2007), (iii) joint modelling of the cluster X-ray gas distribution (e.g. Mahdavi et al. 2007) and (iv) dynamical analysis of the velocity distribution of the stars near the potential centre (e.g. Miralda-Escudé & Babul 1995; Sand et al. 2004; Gavazzi 2005; Koopmans et al. 2006). Despite these important improvements, it is not fully proved that cluster Dark Matter (DM) distribution closely follows the 'universal' profile (Navarro et al. 1997, hereafter NFW) predicted by *N*-body numerical simulations. For this profile, the DM space density is cuspy at the centre ($r \propto r^{-1}$ for $r \lesssim r_{\rm s}$) and behaves as r^{-3} outward. Measuring with great accuracy these two main characteristics is challenging and no consensus has arisen yet with the present-day lensing observations. Recent analysis has shown that Sérsic profile (Merritt et al. 2005) is also fitting the universal mass profile of numerical simulations. Importantly, the mass profile has only a weak dependence on the halo mass or cosmology, allowing to stack different measurements together to improve their significance.

At large radius, analyses of the hot gas distribution from the X-ray observations (Pointecouteau, Arnaud & Pratt 2005; Schmidt & Allen 2007) as well as WL (Kneib et al. 2003) seem to favour an NFW-like profile for galaxy clusters. For elliptical galaxies, Wilson et al. (2001) claimed that they were consistent with isothermal profile out to about 1 Mpc. Also, for massive elliptical galaxies with gravitational rings, Gavazzi et al. (2007) found that the WL slope of the mass density could be $\propto r^{-2}$ out to 300 kpc.

In the core of mass concentrations, the actual existence of a DM cusp predicted by simple numerical simulations is more unclear. For spiral galaxy haloes, the existence of a singular density profile is still

★E-mail: tuhong@shnu.edu.cn

a debate because rotation curves are better explained by isothermal profiles with a core radius (Salucci 2003). Projection effects of non-circular star orbits in triaxial haloes have been invoked, but only in a few cases, to explain the linear increase of the velocity at the centres of galaxies (Hayashi & Navarro 2006). As a consequence, various mechanical processes, such as gas cooling, supernova and active galactic nuclei (AGN) feedback, binary super massive black holes, dynamical friction of the gas outflow during AGN activities, were investigated to explain the formation of a DM core radius (Peirani, Kay & Silk 2006, and references therein). For galaxy clusters, it is often argued that isothermal ellipsoid mass distributions with a flat core could better match the gravitational arcs geometry than NFW profiles (Gavazzi et al. 2003; Sand et al. 2004; Gavazzi 2005). X-ray observations generally do not help much for this issue because, due to the limited spatial resolution of X-ray telescopes, one can just place upper limits on the radius of the smallest DM core, around 30–50 kpc (Chen et al. 2007). In summary, the DM density profile is still an open question, and high-quality data are necessary to settle these questions.

The deviation of light by masses is well described by gravitational lensing effect deduced from general relativity theory. The exquisite *Hubble Space Telescope* (*HST*) images (particularly from the now defunct ACS camera) are providing the necessary lensing constraints to model observed gravitational lensing systems and may directly probe the existence of a 'universal' density mass profile. However, one has to struggle to fully take into account the many observational parameters entering a lens modelling.

First, it is difficult to assess the stellar mass contribution because the stellar mass-to-light ratio (M/L) is generally badly determined, as well as the number of subhaloes and their galaxy occupation numbers (Wright & Brainerd 2002). Secondly, lens modelling only probes the projected mass distribution of lenses along the line of sight which introduces degeneracies in the 3D density profile if the mass profile is only determined on a small range of radius. When testing parametric models of mass distributions for a given DM condensation, these current difficulties are only partly alleviated if we can probe the projected mass at many different radius. As an example, to disentangle between a flat core or a cusp with strong lensing it is not enough to detect and analyse gravitational images very close to the centre, the so-called demagnified central images (Gavazzi et al. 2003) or inner radial arcs (Mellier, Fort & Kneib 1993; Comerford et al. 2006). Even in such ideal cases, some information on the mass distribution beyond the Einstein radius is also critically needed. Beyond giant arc radii, one can use the information in the distortion of singly highly magnified arclets, in an intermediate shear regime ($2 < \mu < 3$), also called flexion regime (Bacon et al. 2006; Massey et al. 2007). However, a generic difficulty similar to the one encountered in the WL needs to be overcome. We do not know the shape of background sources and the flexion method must be used in a statistical way. Only with the most deepest space-based observations, it becomes possible to reach surface number density of background galaxies large enough to conduct such analysis on a single cluster (see recent work on Abell 1689 by Leonard et al. (2007), where they reach a density of background sources equal to $\sim$200 sources arcmin^{-2}).

From the above discussion, we understand the difficulty to conduct an accurate measurement of the slope of the 3D density profile at large radial distances. Hence, considering new probes of cluster mass profile is important.

In this paper, we propose a method to investigate the slope of cluster mass profiles. Gravitational image systems, i.e. 'rings' formed around galaxy cluster members, are used to analyse the slope of the cluster's density profile. Nowadays, such rings can be systematically searched with dedicated software (e.g. Gavazzi et al., in preparation; Cabanac et al. 2005). Here, we outline the method with three rings detected around Abell 1689. The main goal is to provide some constraints on the cluster potential at the location of the rings (i.e. at $\sim$100 arcsec from the centre of the brightest cluster galaxy). The coordinate system in this work is centred on the brightest cluster galaxy: $\alpha_{J2000} = 13{:}11{:}29.52, \delta_{J200} = -01{:}20{:}27.59$.

The paper is organized as follows. First, we rapidly summarize the properties of gravitational rings observed in the field around elliptical lenses. In Section 3, we illustrate the method by using simulated cluster profiles, lensing galaxies and resulting images. These simulations show that we can put constraints on the local slope of the projected mass distribution. In Section 4, the method is applied to Abell 1689. In this case, we show that the three rings confirm that the cluster is dominated by a bimodal mass distribution and that the local slopes of both clumps are not much steeper than isothermal. Then, the results are discussed relatively to previous lensing models of Abell 1689, including a WL analysis in the field of the rings. Finally, we conclude that this method should be better used on very relaxed clusters (single halo) with regular geometry to better probe the slope of the mass profile at various distances from the cluster centre.

Throughout this paper, we assume a cosmological model with $\Omega_m = 0.3, \Omega_\Lambda = 0.7, H_0 = 70\,\mathrm{km\,s^{-1}\,Mpc^{-1}}$. At the redshift of the cluster Abell 1689 ($z = 0.185$) 1 arcsec is equivalent to 3.089 kpc.

2 RINGS AROUND ELLIPTICAL GALAXIES

The number of gravitational rings in the sky is large (Miralda-Escudé & Lehar 1992). Observations of strong lensing in the COSMOS field (Faure et al. 2008) have confirmed the estimation of their surface number density in optical survey (about 10 deg^2 with an average Einstein radius of about 0.8–1.″5). With the development of large surveys like the Sloan Digital Sky Survey (SDSS) and more recently the CFHTLS (http://www.cfht.hawaii.edu/Science/CFHLS/), several hundreds of such arc systems are currently being discovered (Cabanac et al. 2007; Bolton et al. 2006). Almost all of them are multiple images of background galaxies found around massive ellipticals. Robot softwares are finding many of them among millions of objects in wide-field optical surveys and can then be studied in details with dedicated follow-up with *HST* or adaptive optic systems (Marshall et al. 2007). Future space-borne surveys like JDEM/SNAP will allow us to discover as many as tens of thousands (Marshall, Blandford & Sako 2005).

Several structural properties have already been derived from the studies of elliptical lenses detected in the SDSS survey (Koopmans et al. 2006; Treu et al. 2006). It has been found that (i) the stellar mass is dominant within the Einstein radius and the velocity dispersion of stars almost matches the velocity dispersion of the lens model ($\sigma/\sigma_{\rm lens} = 1.01 \pm 0.02$ with 0.065 rms scatter); (ii) the orientation of DM coincide with the light distribution within the Einstein radius and (iii) the best fit for strong lens models coupled to a dynamical analysis of the star velocity dispersion demonstrates that an isothermal profile with $\rho \propto r^{-2\pm0.13}$ can describe the total mass distribution at the Einstein radius.

For elliptical galaxies in clusters, one can expect that the light distribution does not provide such a good geometrical description of the mass distribution. According to simulation (Limousin et al. 2007c), the stellar contribution to the total mass is larger for galaxies in the cluster core. Indeed, as galaxies are crossing the higher density region of the cluster, the DM halo component is tidally stripped

up to a radial distance which is not much larger than the galaxy optical size. This halo stripping has been studied observationally by galaxy–galaxy lensing investigations. Although the deflection caused by galaxy scale mass concentrations is small (i.e. shear $\gamma \sim 0.01$), it is measured in many clusters (Natarajan et al. 1998; Geiger & Schneider 1999; Natarajan, Kneib & Smail 2002a; Natarajan et al. 2002b; Limousin et al. 2007a) and there is a clear evidence for truncation of galaxy DM haloes in the higher density environments. The inferred average half mass radius is found around 40 kpc in cluster cores, whereas half mass radii larger than 200 kpc are derived for field galaxies of equivalent luminosity (see Limousin et al. 2007a, for a review of galaxy–galaxy lensing studies). Hence, the DM mass and stellar mass can be of the same order within the ring. However, in the following, we will only consider a total mass modelling of the ring.

The recent SL2S survey (http://www.cfht.hawaii.edu/∼cabanac/SL2S/) shows that the lens modelling of 'ring' often requires the contribution of an external shear that are likely produced by nearby galaxy groups. In the outskirts of massive cluster, it is also very likely that 'rings' are present and strongly affected by the cluster shear (Smail et al. 2007). For example in the *HST*/ACS images of Abell 1689, several rings have been found (Limousin et al. 2007b).

3 SIMULATIONS OF CLUSTER RINGS

Cluster mass profiles can be described by different models such as the NFW mass profile, a truncated cored isothermal model (Kneib et al. 1996) or a cored power law (Kneib et al. 2003; Broadhurst et al. 2005). The latter two models are defined by three parameters whereas NFW is only defined by two parameters. For simple simulations, we have chosen to describe the cluster mass profile by a single DM clump parametrized by a cored power-law profile. The slope and core radius of the power law are chosen in such a way that it can produce giant arcs at $R_e \sim 45$ arcsec similarly as in Abell 1689. Ideally, the radius over which we will find rings should be significantly larger than the core radius r_c so that the slope of the mass profile is almost constant at the radius of the 'ring'. For a cored power law, the 3D density can be written as

$$\rho(r) = \rho_0 \left(1 + \frac{r}{r_c}\right)^{-n}, \tag{1}$$

so that the logarithmic slope of the 3D mass density ρ is given by n.

Then, on top of this smooth cluster DM component we add a galaxy at a distance R from the cluster centre and we form a 'ring' by lensing a distant galaxy. We then consider as constraints *only* the multiple images generated as part of the ring(s). In order to reproduce the astrometric accuracy of the *HST*–ACS images,we add random errors for the position of the multiple images ($\pm 0\overset{''}{.}05$ rms). In the following, these artificial observations are then used to probe the slope n of the cluster potential without considering any additional giant arcs. Different observational configurations are investigated with one similar to the Abell 1689 observation discussed later.

We will investigate the results on the measurement of n as a function of the ring distance to the cluster centre, and as a function of n. All the simulations were done using the LENSTOOL software (described in Jullo et al. 2007) that allows to easily investigate the important model parameters and their degeneracies by using a Bayesian approach.

The rings in our simulations are described by a truncated isothermal profile for the total mass (pseudo-isothermal mass distribution, hereafter PIEMD; Kassiola & Kovner 1993; Brainerd, Blandford & Smail 1996; Limousin, Kneib & Natarajan 2005)

$$\rho(r) = \frac{\rho_0}{\left(1 + r^2/r_{\rm core}^2\right)\left(1 + r^2/r_{\rm cut}^2\right)} \tag{2}$$

with an ellipticity of the total mass [$\epsilon = (a^2 - b^2)/(a^2 + b^2)$] and position angle (PA) of the halo follow those of the light. In all simulations, the cluster centre is set at ($x = 0$, $y = 0$) coordinates.

3.1 Case A: single ring configuration

3.1.1 Optimizing (n)

To investigate with which accuracy we can recover the slope of the mass profile of the cluster, we have produced different mock configurations by varying the slope ($n_{\rm IN}$) and generating multiple images around the lensing galaxy. Then, we optimize the slope of the cluster mass profile using these multiple images as constraints to estimate ($n_{\rm OUT}$). With only one 'ring', the maximum number of free parameters available is three for a triple image system and five for a quadruple image system.

For the ring we can either choose σ or $r_{\rm cut}$. In principle, the velocity dispersion $\sigma_{\rm ring}$ can be measured from high-resolution spectroscopy of the stellar component, so when there are only three parameters available, we thus choose to optimize $r_{\rm cut}$. Besides, the cluster slope n and the velocity dispersion $\sigma_{\rm cl}$ of the Power Law potential

$$\phi(r, \theta) = 6\pi \frac{\sigma_{\rm cl}^2}{c^2} \frac{D_{LS}}{D_S} r_0 (1 + (r/r_0)^2 \{1 + \epsilon \cos[2(\theta - \theta_0)]\})^{(3-n)/2} \tag{3}$$

are the parameters we will optimize, as the other ones (centre, geometry, core radius) should be well known from the modelling of the cluster multiple images. As our preliminary goal is to see how well in this simplest simulation we can recover the input slope ($n_{\rm IN}$) of the cluster, we present the analysis for three different geometric configurations of the lensing galaxy: (i) galaxy halo without any ellipticity; (ii) galaxy halo with an ellipticity of 0.2 and position angle (PA) = 0° with respect to the line connecting the ring to the centre of the cluster (radial configuration) and (iii) galaxy halo with an ellipticity of 0.2 and PA varying up to 90° (orthoradial configuration).

Results of the simulations and modelling are shown in Fig. 1. We have verified that the ellipticity and orientation of the lensing galaxy relative to the cluster shear do not change the accuracy in the recovering of the slope n. We plot the results for a fixed initial cluster velocity dispersion to show that the shallower the profile, the better the recovery of the slope. Indeed, the shallower the profile, the more massive the cluster, and thus stronger its influence on a ring galaxy located at a fixed radius.

3.1.2 Dependence with radial distance $R_{\rm ring}$

When optimizing n, we have fixed the rings to be at 100 arcsec from the cluster centre because it corresponds to the radius of rings we have found in the field of Abell 1689. Finding rings further away from the critical region, where the shear of the cluster becomes weaker may bring interesting constraints on the cluster mass profile. To investigate this possibility with wider field survey of clusters, we have conducted simple simulation varying the ring radial distance from 100 to 300 arcsec to see how well we can recover the local cluster mass profile. Results are shown in Fig. 2. The improvement in the determination of the slope does not depend on the azimuthal distribution of the ring around the cluster. But indeed if several rings are aligned on a same direction, we cannot use them to estimate the cluster centre (see Section 3.1.3).

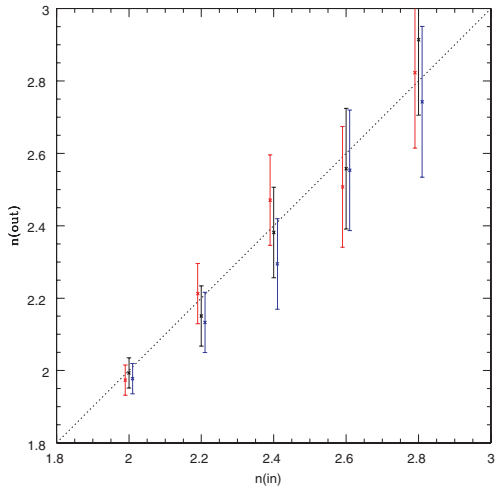

Figure 1. Results for a single ring configuration. The ring is located 100 arcsec from the cluster centre. The deformations are generated using a power-law profile whose slope is $n_{\rm IN}$ reported on the horizontal axis. Using the constraints provided by the rings, we estimate this slope $n_{\rm OUT}$ which is reported on the vertical axis. The black points with errorbars correspond to a sample of single ring around a circular galaxy, the red points to a radial configuration and the blue points to an orthoradial configuration. The black dashed line denotes the equality.

At distance larger than ∼300 arcsec (≃ 1 Mpc), as the cluster influence is getting small, it is only possible to give a lower limit on the slope n. None the less, such a result can be useful as it would show that the slope of the mass profile has departed from the isothermal slope ($n = 2$). This can be understood if we consider the total convergence κ which is encompassed within the ring radius R (ring). It comes from the contribution of the galaxy and the cluster ($\kappa = \kappa_{\rm G} + \kappa_{\rm cluster}$). The convergence of the galaxy $\kappa_{\rm G}$ cannot be arbitrarily high, also the optimization cannot accommodate any shallow cluster profile that will give a cluster contribution $\kappa_{\rm cluster}$ which is too high, since $\kappa_{\rm G} + \kappa_{\rm cluster} \simeq 1$. The better the likelihood on $\kappa_{\rm G}$, the better will be the determination of n. Also the star velocity dispersion within the ring (total mass) can strongly improve the result. Only at large radius when both $\kappa_{\rm cluster}$ and $\gamma_{\rm cluster}$ become very small variation across the ring, the method reaches its limit (see Fig. 2).

If a cluster has an NFW potential, the logarithmic slope of the NFW mass profile is 'continuously' varying. A power-law approximation with a core can match at the same time the total mass of the cluster within the ring and the local slope, but it results in an unphysical core radius $r_{\rm core}$. Also for real clusters and data set, the best way is to directly test an NFW model for the cluster component by including as many multiple images as one can find (see Section 4).

3.1.3 Finding the cluster centre

In this section, we investigate how to retrieve the location of the cluster centre using several ring systems ∼100 arcsec from the cluster centre. In this exercise, we take the cluster position as two free parameters. As shown in Fig. 3, a single ring cannot reliably find the centre of the cluster but does give some constraints on its direction. Note that the probability distribution contours are large and not centred on (0, 0).

3.2 Case B: multiple rings configuration

We now consider three rings located at 100 arcsec from a cluster centre similarly as observed in Abell 1689. They surround the cluster: one is in the north of the cluster, one is in south and the third one is in west (see Fig. 3). We then conduct the same simulations as done for a single ring but with the three rings.

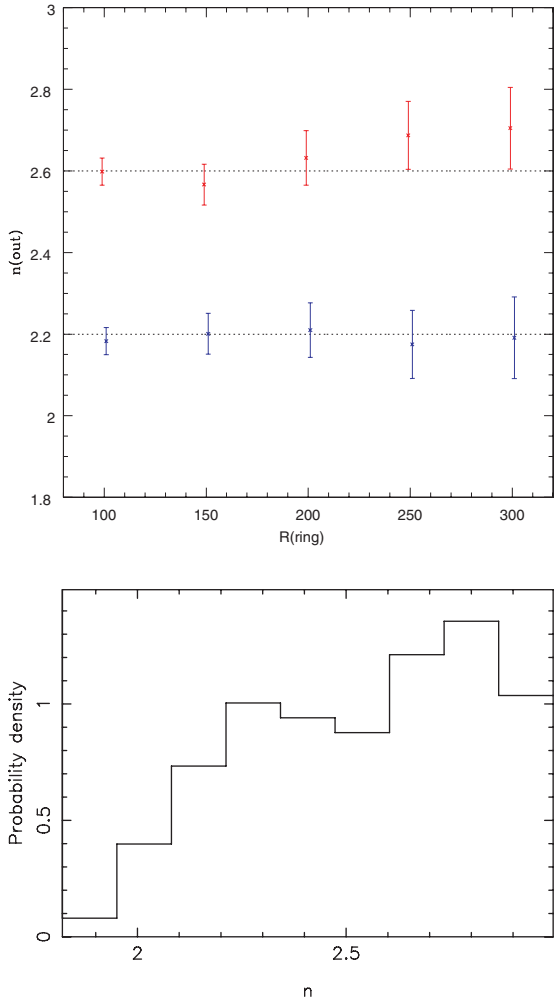

Figure 2. Top panel: dependence of the accuracy of the method with respect to the distance between ring and cluster centre R (ring). In red, the input slope is $n = 2.6$, whereas in blue the input slope is $n = 2.2$. Bottom panel: histogram of the probability density of n values for the point 250 arcsec and $n = 2.6$ taken from the top figure.

Results on recovering the cluster potential slope are shown on Fig. 4. Compared to Fig. 1, we see that having three rings improves the measurement accuracy of the slope following a $\sqrt{3}$ factor.

Regarding the cluster centre, we recover the centre of mass with the following accuracy $x = 0 \pm 50$ arcsec and $y = 0 \pm 50$ arcsec. The constraints on the position of the clump are shown in Fig. 3. This measurement is not very accurate comparing to what we can achieve by analysing giant arcs systems generated by a cluster. However, the simulation shows that not only the rings are sensitive to the slope of the potential, but also if we have enough rings, we can guess whether the location of the mass centre really dominated by a single massive clump.

3.3 Conclusions from simulations

A single ring can provide a good constraint on the slope of the cluster mass profile beyond its Einstein radius because the modelling constrains at the same time the local value of cluster convergence

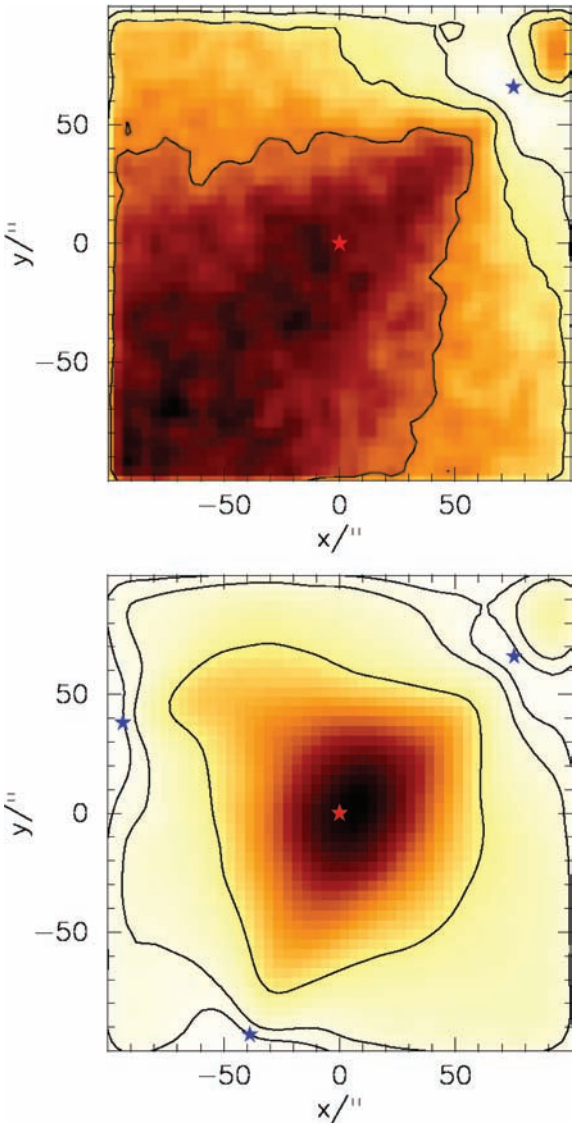

Figure 3. Recovering the cluster position using the constraints provided by the ring(s). Top panel: one ring (labelled by a blue star) is located at 100 arcsec from the centre of the cluster (red star). Bottom panel: similar results but with three rings (blue stars) located at ∼100 arcsec. The contours define the 1σ, 2σ and 3σ region.

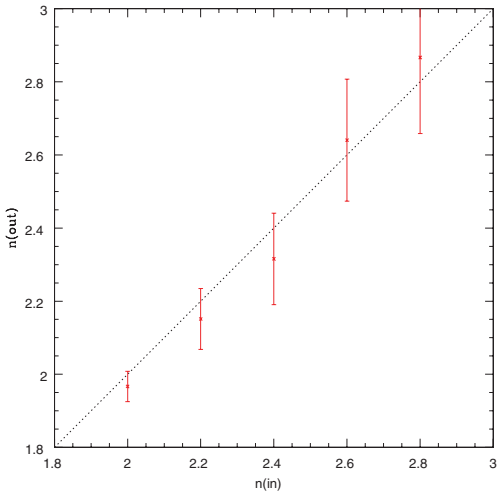

Figure 4. Results for a three ring configuration similar to Abell 1689. The rings are located 100 arcsec from the cluster centre and surround the main clump. The deformations are generated using a power-law profile whose slope is $n_{\rm IN}$ reported on the horizontal axis. Using the constraints provided by the rings, we measure the slope $n_{\rm OUT}$.

and shear. Schematically outlined, we can say that the cluster convergence enlarges the Einstein radius of the ring and the shear rotates and changes the ellipticity of the critical line. Since both the convergence and the shear depend on the slope n at the location of the rings ($R = R_{\rm ring}$), the simultaneous adjustment of $\kappa_{\rm cluster}$ and $\gamma_{\rm cluster}$ provides a determination of n. The ring method can probe at which distance the slope of a cluster potential departs from $n = 2$ (isothermal slope). Using simulations, we are finding that there is a large range of cluster radii ($R_{\rm e} < R < 10\ R_{\rm e}$) over which rings can efficiently probe the mass profile slope. An optimum case would be to observe rings at various cluster-centric distances to better probe the overall DM profile.

The ring method cannot put strong constraints on the position of the clump perturbation. The centre of the clump should be determined independently to take full advantage of the method (centre from X-ray or giant arc modelling). However, it can give information on the clumpiness of the DM distribution since each ring is more sensitive to its closest DM clump. With many rings surrounding a single dominant cluster potential, one can measure more accurately the slope of the mass profile, as well as determine the centre of mass.

4 APPLICATION TO ABELL 1689

With more than 31 arc systems, Abell 1689 (one of the richest clusters of galaxies at intermediate redshift) is producing the largest number of strong lensing images. Although, the X-ray map looks circular and is centred on the brightest cluster galaxy (BCG), there is no cool core and the gas has complicated dynamics (Andersson & Madejski 2004). Furthermore, the line-of-sight velocity dispersion is complex (Girardi et al. 1997; Łokas et al. 2006). Broadhurst et al. (2005) found that the multiple arc systems can be modelled with a power-law potential with $n \simeq 3.08$, a surprisingly steep potential. As we will show below the three rings do not support a single power-law potential.

In fact, the most recent strong lensing models show a bimodal mass distribution (Miralda-Escudé & Babul 1995; Halkola, Seitz & Pannella 2006; Leonard et al. 2007; Limousin et al. 2007b). The cluster can be described as a dominant central DM mass clump (O1 in the following) and a smaller perturbation associated with the north-east galaxy group (O2 in the following). Although this two mass clump description is not fully satisfactory (see discussion in Limousin et al. 2007b), it can be considered as a first-order approximation for the analysis presented here. Despite its complexity, we will apply the method presented above on Abell 1689. Furthermore, Abell 1689 has been extensively studied, allowing us to compare our results to former studies as a check for the ring method.

In the following analysis, we will explore if the constraints provided by these three rings can probe the bimodality of the mass distribution, as well as the slope of each clump at the location of the rings (about 100 arcsec corresponding to 300 kpc from the centre) without any strong a priori assumptions coming from previous arc modelling. Next, we will use the results of previous modelling as

input parameters to check if they remain compatible with the ring configuration.

4.1 Ring constraints

Fig. 5 shows the whole ACS field of view with the location of the three rings, as well as three panels corresponding to each ring. The three rings in Abell 1689 are at ∼100 arcsec (≃ 300 kpc) from the cluster centre surrounding the two main luminous components (Table 1).

The three lensing galaxies are cluster members (based on their redshift) and have similar colour as the cluster red sequence. The lensed blue features around the ring G3 have a measured spectroscopic redshift of $z = 1.91$ from LRIS at Keck (Richard et al. in preparation). For the other lensed features around G1 and G2, we will assume for simplicity a redshift $z = 1$. As a consequence, the velocity dispersion that we will derive has a loose meaning because of the assumption on the lensed redshift. The constraints we are considering here are only those derived from the blue-lensed features detected around each ring (see Fig. 5). For a system with N multiple images, we get $2(N - 1)$ constraints. Therefore, these give us a total of 16 constraints (Table 1).

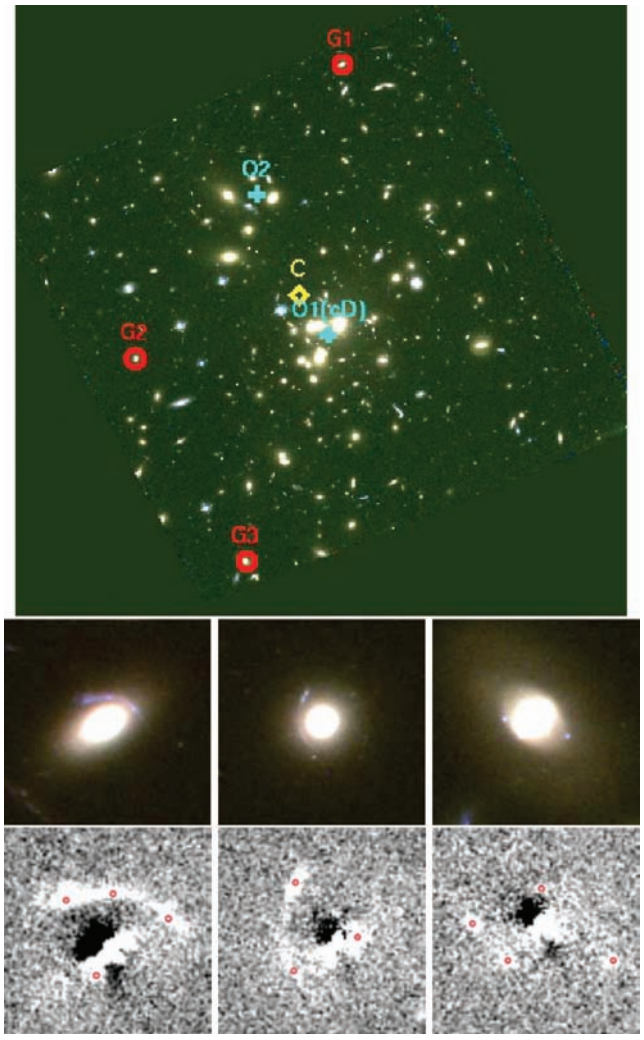

Figure 5. Galaxy cluster Abell 1689. The field size is 280 × 280 arcsec^2, corresponding to 1089 × 1089 kpc. G1, G2 and G3 are the three rings involved in this work. The images with lens galaxies subtracted are in the bottom row. The images we use as constraints are marked as little red circles. The diamond (C) is the optimized centre of the potential in the model we find with a single potential. It goes to the direction of the luminous clump in the north east (labelled by a cross O2). The centre found by X-ray is marked by a cross (O1).

In the following, we *only* use these 16 constraints in order to probe the cluster without any a priori coming from the arc systems. The LENSTOOL reduced χ^2 quantifies how well we reproduce the location of the gravitational ring images for each family of lens models. To describe each ring system, we use a PIEMD profile for which we fix the position, ellipticity and PA according to the light distribution. Then, we optimize the velocity dispersion σ and cut-off radius $r_{\rm cut}$ for each ring. For ring G3, we also optimize the core radius $r_{\rm core}$ to ensure a better match with this special lensing configuration although this has only a very minor impact on the results presented below. So in total, we use seven free parameters to describe the three rings. This lets us enough degrees of freedom (d.o.f.) to explore some cluster properties.

4.2 Bimodality of the cluster mass distribution

If the central mass distribution of Abell 1689 is bimodal, the ring configuration will be different as compared to the one in a single central potential. The local external shear at each ring location has another direction. We have tried to simultaneously model the three rings with only one single central potential of either singular isothermal sphere (SIS), NFW or power-law profile for which we optimize the position of the centre and the dynamical parameters. We find that the χ^2 per d.o.f. is always larger than 100!

During this inconclusive optimization, LENSTOOL favours the centre of the potential to be between O1 and O2 (Fig. 5). This is unlikely since we know from both the lens model of the arcs and the X-ray map that most of the mass is centred on the BCG.

Thus, we introduced a second mass component in the model. We fix all the parameters of the main mass component O1 to the values found in previous modelling (centred on the BCG), and we let free the location and the velocity dispersion of the second mass component. Much better solutions are found in this case, with a reduced χ^2 smaller than 4. In previous parametric strong lensing studies, the position of the second mass component is not well constrained. In this study, we find a value [RA = 13:11:31.360 ± 7 (arcsec), y = −01:20:04.66 ± 21 (arcsec)] close to the light centre of O2. This test confirms that the three rings are sensitive to the bimodality of the cluster central mass distribution, thus providing an extra evidence for bimodality in this cluster.

4.3 The slope of the mass distribution

4.3.1 Cluster modelling and rings

The three rings are sensitive to the Abell 1689 gravitational field and, in principle, we can use them to constrain the local slope of the potential at the location of the rings. With the constraints of three rings, we cannot explore too many parameters. Also, we first assume that each mass component O1 and O2 can be described by a power-law profile with a core radius. Thus, we fix the position of clump O1 to coincide with its brightest galaxy, and the position of clump O2 with the barycentre of its brightest galaxies. We also fix the ellipticity and PA according to the cluster arcs modelling of (Halkola et al. 2006) (Table 2). The only free parameters which are left free are the slope and velocity dispersion for each mass clump (six parameters for the two clumps). As discussed in

Table 1. Strong galaxy–galaxy lensing events involved in this work: coordinates (J2000), distance to the BCG; spectroscopic redshift measurements when available; *F775WAB* magnitudes obtained from the surface brightness profile fitting by (Halkola et al. 2006); circularized physical half light radius in units of kpc (Halkola et al. 2006); redshift of images; number of constraints provided by these images.

Number	RA	Dec.	$d_{\rm BCG}$ (arcsec)	Lens $z_{\rm spec}$	Lens magnitude	$R_{\rm e}$(kpc)	Images z	Number of constraints
1	197.872	−1.309	114	0.1758	18.25 ± 0.13	2.0 ± 0.1	1.0 (assumed)	6
2	197.897	−1.345	90	0.1844	18.58 ± 0.16	2.2 ± 0.2	1.0 (assumed)	4
3	197.884	−1.369	110	0.1855	18.11 ± 0.01	4.1 ± 0.1	1.91	6

Section 4.1, we have seven parameters to describe the three rings. For the free parameters, the ranges of variation are chosen as follow. The parameters of each ring galaxy can vary between reasonable limits for a galaxy scale potential, i.e. a central velocity dispersion σ_0 between 100 and 300 km s^{-1}, and the cut-off radius between 5 and 100 kpc. The velocity dispersion of each clump is allowed to vary up to 2500 km s^{-1}. The slope n can vary between 1.0 and 3.0. Under these hypotheses, the slope of the potential associated with the main central clump is found to be $n = 2.4^{+0.1}_{-0.4}$, which is a little steeper than an isothermal sphere. But surprisingly a large value of 108 ± 32 arcsec is found for the core radius of O1. It corresponds almost exactly to the distance of the closest rings. Since we prefer to only use a power-law approximation when the core radius is really smaller than the radial ring distance, we try to force the core radius at the value of Halkola et al. 2006 (Table 2). Then, we recover a similar value $n = 2.46^{+0.06}_{-0.60}$ for the main clump but the mass of the second clump O2 becomes larger than the mass of O1. It appears that a larger core radius can match the mass found for each clumps with the modelling of the 31 gravitational arc systems but a small core radius for O2 does not. Clearly, rings seem to tell us that the mass distribution of clump O2 cannot be approximated by a single central potential and that its mass distribution is probably more complex. This can be understood if clump O2 is in fact a projection of a filamentary distribution of mass along the line of sight. We give as an illustration in Table 2 the results of the optimization with the Halkola's core radius values fixed (in brackets). Besides, we will see below that we have a degeneracy of solutions between the velocity dispersion and $r_{\rm cut}$ for each galaxy.

Table 2. Best-fitted parameters for the power-law mass distribution of the two clumps. The parameters in brackets are fixed during the optimization.

Main clumps	Halo one	Halo two	
x (arcsec)	[−2.1]	[−33.1]	
y (arcsec)	[−4.7]	[56.7]	
ϵ	[0.159]	[0.385]	
θ	[56.4]	[106.3]	
$r_{\rm core}$ (arcsec)	[18.13]	[24.28]	
n	$2.46^{+0.06}_{-0.60}$	$2.49^{+0.10}_{-0.27}$	
σ (km s^{-1})	709.15 ± 538.16	1119.97 ± 178.66	
Rings	G1	G2	G3
x (arcsec)	[3.527]	[−86.088]	[−38.581]
y (arcsec)	[113.703]	[−14.64]	[−102.812]
ϵ	[0.492]	[0.09]	[0.443]
θ	[−33.4]	[−24.9]	[43.8]
$r_{\rm core}$ (arcsec)	[0.01]	[0.01]	0.01 ± 0.07
$r_{\rm cut}$ (arcsec)	14.6 ± 16.9	<10	<10
σ (km s^{-1})	173.74 ± 13.99	162.07 ± 23.02	174.70 ± 27.40
Constraints		16	
Free parameters		11	
$\chi^2_{\rm tot}$		18.27	
χ^2/d.o.f.		3.65	

4.3.2 Degeneracies

Parametric strong lensing models with many parameters exhibit various degeneracies. One reason is that strong lensing is sensitive to the projected enclosed mass which is degenerated with respect to some of the parameters describing the 3D mass density. For a discussion on the degeneracies encountered in parametric lens modelling, one can refer the work of Jullo et al. (2007).

In Fig. 6, we present the most relevant degeneracies for the slope of the main clump O1 and the other parameters found in this work. We see that the velocity dispersion and slope n of O1 are poorly constrained as expected. Similar degeneracies are obtained for O2. The bayesian framework in which LENSTOOL proceeds, it is important to specify the meaning of the 'best-fitting model', especially in such cases of strong departs from Gaussianity. Throughout this paper, we define the best-fitting value for a given parameter as the mode of the marginalized distribution (integrated over all other dimensions). Hence, we can see some inconsistency between such values (summarized in Table 2) and Fig. 6 which directly comes from Bayesian techniques. For instance, the high value for the slope n(O1) $= 2.4^{+0.06}_{-0.60}$ is essentially due to the choice of the exploration range for σ(O1). The inferred value for n(O1) would be lower when decreasing the upper limit of the variation range of σ(O1). For comparison, in a more frequentist fashion, one would find values n(O1) $\simeq 1.5$ near the minimum χ^2. Fig. 6 also shows the interest of measuring the velocity dispersion of G1 and clump O1 to break the degeneracy and get valuable constraints on the density slopes.

We have noted that the ring G2 is closest to O1. Therefore, we make a test only with G2 to see if it gives an equivalent result for the slope of O1. Like the single ring simulation in Section 3.1, only the images around G2 are used in the optimization. Now the slope and velocity dispersion of the main clump (O1) and the velocity dispersion of G2 are optimized with only four constraints.

In this case, we take other parameters compatible with three ring modelling. A local slope is found to be equivalent to $n = 2.4 \pm 0.2$. For the second clump, the degeneracies are larger and we found the logarithmic slope could be steeper than 2.4.

Ultimately, one would like to try a simultaneous modelling of the three rings together with the 31 multiple arc systems of Abell 1689. However, this would go beyond the scope of this work for two reasons. First, the description of the second clump is likely to

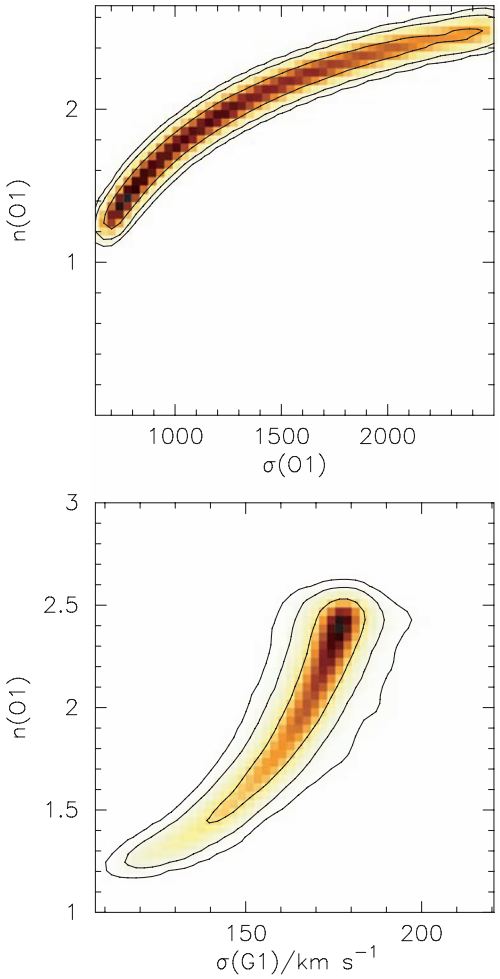

Figure 6. Degeneracies between the slope of the main central clump and dispersion of clump one and G1. The peak value found for the slope parameter is $n = 2.46^{+0.06}_{-0.60}$ (see Table 2). These degeneracies underline the importance in obtaining the velocity dispersion of the clumps and lensed galaxies.

be more complex than previously thought. Secondly, a comprehensive investigation with LENSTOOL would need an enormous amount of computer time just to analyse one of several possible potential configuration. Instead, we can test published models of Abell 1689 to check how well the rings are reproduced (we call this the 'ring test'). To do this, we took as an input the structural parameters of the cluster potential and we only solve for the ring configurations to evaluate the χ^2. As we have already demonstrated above, the power-law model of Broadhurst et al. (2005) does not pass the test at all. For the Halkola et al. (2006) models, the ring test gives a reduced χ^2 of 5.4 for the SIS model and 5.9 for the NFW model, suggesting that the local slope for both case will not depart much from the isothermal solution.

4.4 Conclusions for the Abell 1689 ring tests

A preliminary conclusion is that modelling of the three rings seems to favour slope a bit steeper than the SIS value at a radial distance of 105 arcsec, with $n = 2.4^{+0.06}_{-0.60}$. On the contrary, the best models of the multiple arc systems (current Einstein radius of about 50 arcsec) favour an SIS or an NFW model with a scale radius r_s around 65 arcsec. Indeed, if r_s is not significantly larger than the radius

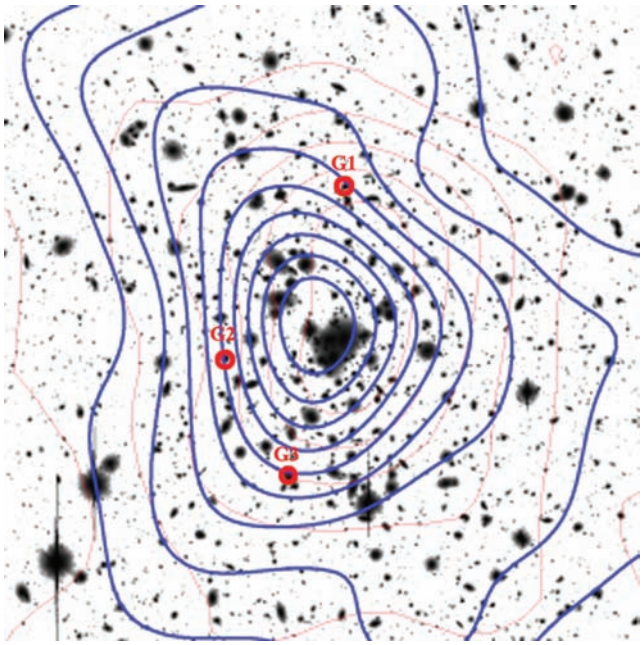

Figure 7. The κ map of Umetsu. The field size is 15 arcmin on a side. Blue contours are the reconstructed lensing convergence κ. The lowest contour and the contour intervals are 0.05. The three rings used in this paper are labelled with red circles. Note that the local slope of κ is remarkably compatible with the slope derived from the ring analysis.

where most of the tangential arc(let)s are formed, the NFW slope remains close to $n = 2$ when $r = r_s$ thus very similar to an SIS model. Abell 1689 rings are at only two times the cluster Einstein radius, and are thus in a situation where we do not expect a strong departure from an SIS slope. Hence, the ring radius R (ring) is not large enough to derive stringent conclusion. Furthermore, the potential complexity of Abell 1689 is likely increasing the degeneracies of the solutions. In the following, we will try to discuss these results and their compatibilities with a WL analysis of Abell 1689.

4.5 Discussions

The lensed features around the three rings contain extra information on the mass distribution and mass profile of the cluster at a distance larger than the tangential arcs. Rings confirm the Abell 1689 bimodality, they also show that the slope of the mass distribution departs from isothermality at 100 arcsec from the cluster centre.

The three rings are located at $R_{\rm ring} \sim 105$ arcsec from the cluster centre. Considering that the dominant cluster mass profile can be characterized by the parameters of O1 only, which is legitimate given the difference in velocity dispersion between each component, we find the slope of the 3D mass density to be equal to $-2.4^{+0.06}_{-0.60}$. Describing Abell 1689 with an NFW profile, this sets an upper limit on the scale radius r_s of the NFW profile: $r_s < R_{\rm ring}$. This upper limit on the scale radius can be compared with the WL analysis of Abell 1689. Limousin et al. (2007b) found both the strong and the WL regime to agree in this cluster. From the Canada–France–Hawaii Telescope (CFHT) data, they pursued a WL analysis, and found a scale radius $r_s = 93$ arcsec. This value agrees with the upper limit provided by the ring constraints. We can eventually try to go a bit further in this comparison between the ring results and the shear map

of Abell 1689. Umetsu, Takada & Broadhurst (2007) have obtained deep images of Abell 1689 with the Subaru telescope and published a projected mass reconstruction. From their fig. 4 (see Fig. 7), we can see that their main centre is almost the centre C determined by the three rings (Fig. 5). Moreover, it is possible to estimate from their map the local slope $n - 1 = -\Delta\log(\kappa)/\Delta\log(R)$ at the location of the three rings. We recover for G1, G2 and G3 an equivalent value of n, respectively, equal to $1.95 \pm 0.2, 2.48 \pm 0.1$ and 2.21 ± 0.2. Although such a rough calculation of the slope is only valid for power-law mass distribution, it seems compatible with the ring analysis. G2 is the closest ring to the centres of the two clumps and the slope obtained from G2 (2.4 ± 0.2, see Section 4.3.2) is similar to the Umetsu et al. (2007) result. We can thus argue that a ring can bring similar information as WL analysis but at a fixed point.

In summary, we found evidence for departure from isothermality at 100 arcsec from the cluster centre (Fig. 6), especially for the G2 location which is not perturbed by outside subclumps. Our results are not in disagreement with previous lens modelling of Abell 1689. We found, in particular, that at the G2 location, the potential is steeper than isothermal.

The three ring galaxies do have a similar $F775W$ magnitude, between 18.11 and 18.58. It is interesting to note that the modelling already infers comparable velocity dispersions values, around $170\,\mathrm{km\,s^{-1}}$, and small cut-off radii. For rings G2 and G3, the cut-radii are found smaller than 10 arcsec. These central galaxies may be highly truncated, in good agreement with the tidal stripping scenario (Limousin et al. 2007c). To investigate further the exact value of cut-off radii, it is necessary to wait for good measurement of the stellar velocity dispersion within the ring radius.

5 CONCLUSIONS

This work revisits the importance of external shear perturbations for the modelling of galaxy lenses (see Dye et al. 2007). But instead of focusing our attention on the improvement of the ring modelling by introducing an external shear, we probe the gravitational potential slope in the outskirts of groups and clusters of galaxies, thanks to the high sensitivity of the ring modelling both to the local external shear and convergence of the cluster. We test the principle of the method with simple simulations using power-law models to describe the cluster mass clumps. From this simulation, we found that within the astrometric accuracy of ACS images a ring can be used to detect a logarithmic slope of the external mass density distribution up to about $n = 2.8$. For an NFW profile with a typical concentration parameter $C_{\rm vir} \sim 5$ (Comerford & Natarajan 2007), this should allow to probe the cluster potential up to a large fraction of its virial radius. It is now possible to detect rings in the outskirts of clusters with new ground-based surveys like CFHT-LS, but the determination of the direction and amplitude of the external shear depends crucially on the high-resolution *HST* images. On the other hand, the knowledge of the lens stellar velocity dispersion and the redshift of the ring itself would increase the robustness to the ring modelling (Koopmans et al. 2006).

Using the three rings found in Abell 1689, we have shown that it is possible to estimate the mass density slope. Hence, we have shown with the information given by rings alone that the potential of Abell 1689 is bimodal. With this limited number of rings it is, however, not possible to better trace other DM substructures within each clump. Therefore, a global modelling of the 31 arcs systems and rings remains a good challenge.

We find a mass density slope a bit larger than $n = 2$ for each DM clump at about 100 arcsec from their centre, but the complexity of the cluster potential really weakens the result. Since the most immediate appealing application of the method is to probe the slope departure from a r^{-2} mass density profile, we strongly suggest similar analysis on less complex clusters. The ideal lenses to probe the reality of a universal NFW profile would be a cluster or a fossil group with a bright cD galaxy having a single dominant halo, and which displays at least a distant ring, a multiple arc with known redshift and a radial arc. Such a configuration would probe the potential at various distances from the centre. The discovery of such 'golden lenses' requests a large survey of massive clusters. Most often clusters with a great number of arcs have multipolar potentials (i.e. longer caustics) so that are more complex to analyse. However, rings are influenced by all their nearby environment (including foregrounds). In this sense, a statistical study of the environmental effect on the rings should be conducted in the future.

Many rings can be discovered now in the field of deep wide-field surveys. It will be possible to improve the method and use it more systematically. As an example, the CFHT-LS 'wide' survey will cover 170°, and we expect to detect about 10 rings per square degree with an average redshift $z_{\rm lens} = 0.65$ (Cabanac et al. 2007). The clusters and groups in front of or at the same redshift as the lensing galaxies have approximately the same sky density (Oguri, Umetsu & Futamase 2006). Thus, we can expect that several rings per square degree will be influenced by the external shear of a nearby mass condensation in the field. Such cases are already observed in the SL2S survey (Cabanac et al. 2007).

For Abell 1689, we have found three rings within the small *HST* field ($r \sim 100$ arcsec), which may be consider as surprisingly high number. In fact, the large number of ellipticals in this cluster and the extra convergence that it adds to the lensing effect most probably compensate for the small field of view imaged with the ACS camera. [1] We also found two possible rings closer to the critical region of Abell 1689 (i.e. at radii smaller than 50 arcsec). However, we are not considering these rings here, because these systems are in a crowded region and cannot be described by a simple contribution of a galaxy and a cluster scale component. Any attempt of modelling these latter rings must involve all the multiple arc systems of Abell 1689. In wide-field surveys, perturbing clusters may be found at a lower redshift than the ring-producing elliptical lenses (e.g. Smail et al. 2007). In such cases, a proper analysis requires a multiplan ring modelling.

In conclusion, rings seem to be a promising tool to constrain the mass distribution slope at large radii from the centres of groups, and clusters provided dedicated observations are carried out on a few golden lenses. They can provide information on many structural parameters of haloes of clusters and galaxies. In complement to the modelling of the multiple arcs in the cluster core, they can confirm or otherwise dispute the existence of the universal DM halo profile predicted by numerical simulation, as well as to study subhaloes and their cut-off radii. For these studies, it is crucial to measure the velocity dispersion of the lens galaxies which produce the gravitational ring images. It clearly appears from the study of Abell 1689 that this method should be implemented first on a sample of very relaxed clusters or (fossil) groups in order to analyse a single DM potential with the simplest possible geometry. Only when large sample of rings is available, it will become possible to start a systematic analysis of the external shear perturbation on ring shapes

[1] After the submission of this paper, King (2007) has shown with cluster simulation that the ring cross-section is increased by a factor of about 3 near critical lines.

in correlation with more complex nearby (eventually foreground) environment.

ACKNOWLEDGMENTS

The authors are very grateful to Raphael Gavazzi for very helpful discussions and comments on the paper. This project is partly supported by the Chinese National Science Foundation No. 10333020, 10528307, 10778725, 973 Program No. 2007CB815402 and Shanghai Science Foundations, and this work was undertaken within the frame of the French 'Agence Nationale de la Recherche' (ANR) project BLAN06-3_135448. HT acknowledges the financial support of the Shanghai Science Foundation for a visit to IAP and is grateful to the hospitality during the visit. HT also acknowledges the Dark Cosmology centre for their invitation in Copenhagen where part of this work has been carried out. The Dark Cosmology Centre is funded by the Danish National Research Foundation. JPK acknowledges support from CNRS. This work is based on observations made with the NASA/ESA *Hubble Space Telescope*, obtained through the archives of the Space Telescope Science Institute, which is operated by the Association of Universities for Research in Astronomy, Inc., under NASA contract NAS 5-26555.

REFERENCES

Andersson K. E., Madejski G. M., 2004, ApJ, 607, 190
Bacon D. J., Goldberg D. M., Rowe B. T. P., Taylor A. N., 2006, MNRAS, 365, 414
Bolton A. S., Burles S., Koopmans L. V. E., Treu T., Moustakas L. A., 2006, ApJ, 638, 703
Brainerd T. G., Blandford R. D., Smail I., 1996, ApJ, 466, 623
Broadhurst T., Takada M., Umetsu K., Kong X., Arimoto N., Chiba M., Futamase T., 2005, ApJ, 619, L143
Cabanac R. A., Valls-Gabaud D., Jaunsen A. O., Lidman C., Jerjen H., 2005, A&A, 436, L21
Cabanac R. A. et al., 2007, ApJ, 461, 813
Cacciato M., Bartelmann M., Meneghetti M., Moscardini L., 2006, A&A, 458, 349
Chen Y., Reiprich T. H., Böhringer H., Ikebe Y., Zhang Y.-Y., 2007, A&A, 466, 805
Comerford J. M., Natarajan P., 2007, MNRAS, 379, 190
Comerford J. M., Meneghetti M., Bartelmann M., Schirmer M., 2006, ApJ, 642, 39
Doré O., Bouchet F. R., Mellier Y., Teyssier R., 2001, A&A, 375, 14
Dye S., Smail I., Swinbank A. M., Ebeling H., Edge A. C., 2007, MNRAS, 379, 308
Faure C., Kneib J. P., Conone G., Tasca L., Leauthaud S., Capak P., Jahnke K. et al., 2008, ApJ, in press
Gavazzi R., 2005, A&A, 443, 793
Gavazzi R., Fort B., Mellier Y., Pelló R., Dantel-Fort M., 2003, A&A, 403, 11
Gavazzi R., Treu T., Rhodes J. D., Koopmans L. V. E., Bolton A. S., Burles S., Massey R. J., Moustakas L. A., 2007, ApJ, 667, 176
Geiger B., Schneider P., 1999, MNRAS, 302, 118
Girardi M., Fadda D., Escalera E., Giuricin G., Mardirossian F., Mezzetti M., 1997, ApJ, 490, 56
Halkola A., Seitz S., Pannella M., 2006, MNRAS, 372, 1425
Hayashi E., Navarro J. F., 2006, MNRAS, 373, 1117
Jullo E., Kneib J.-P., Limousin M., Elíasdóttir A., Marshall P., Verdugo T., 2007, New J. Phys., 9, 447
Kassiola A., Kovner I., 1993, ApJ, 417, 450
King L. J., 2007, MNRAS, 382, 308
Kneib J.-P., Ellis R. S., Smail I., Couch W. J., Sharples R. M., 1996, ApJ, 471, 643
Kneib J. et al., 2003, ApJ, 598, 804
Koopmans L. V. E., Treu T., Bolton A. S., Burles S., Moustakas L. A., 2006, ApJ, 649, 599
Leonard A., Goldberg D. M., Haaga J. L., Massey R., 2007, ApJ, 666, 51
Limousin M., Kneib J.-P., Natarajan P., 2005, MNRAS, 356, 309
Limousin M., Kneib J. P., Bardeau S., Natarajan P., Czoske O., Smail I., Ebeling H., Smith G. P., 2007a, A&A, 461, 881
Limousin M. et al., 2007b, ApJ, 668, 643
Limousin M., Sommer-Larsen J., Natarajan P., Milvang-Jensen B., 2007c, preprint (arXiv:0706.3149)
Łokas E. L., Prada F., Wojtak R., Moles M., Gottlöber S., 2006, MNRAS, 366, L26
Mahdavi A., Hoekstra H., Babul A., Sievers J., Myers S. T., Henry J. P., 2007, preprint (astro-ph/0703372)
Marshall P., Blandford R., Sako M., 2005, New Astron. Rev., 49, 387
Marshall P. J. et al., 2007, ApJ, 671, 1196
Massey R., Rowe B., Refregier A., Bacon D. J., Bergé J., 2007, MNRAS, 380, 229
Mellier Y., Fort B., Kneib J.-P., 1993, ApJ, 407, 33
Merritt D., Navarro J. F., Ludlow A., Jenkins A., 2005, ApJ, 624, L85
Miralda-Escudé J., Lehar J., 1992, MNRAS, 259, 31
Miralda-Escudé J., Babul A., 1995, ApJ, 449, 18
Natarajan P., Kneib J.-P., Smail I., Ellis R. S., 1998, ApJ, 499, 600
Natarajan P., Kneib J.-P., Smail I., 2002a, ApJ, 580, L11
Natarajan P., Loeb A., Kneib J.-P., Smail I., 2002b, ApJ, 580, L17
Navarro J. F., Frenk C. S., White S. D. M., 1997, ApJ, 490, 493
Oguri M. et al., 2006, AJ, 132, 999
Okura Y., Umetsu K., Futamase T., 2007, preprint (arXiv:0710.2262)
Peirani S., Kay S., Silk J., 2006, preprint (astro-ph/0612468)
Pointecouteau E., Arnaud M., Pratt G. W., 2005, A&A, 435, 1
Salucci P., 2003, preprint (astro-ph/0310376)
Sand D. J., Treu T., Smith G. P., Ellis R. S., 2004, ApJ, 604, 88
Schmidt R. W., Allen S. W., 2007, MNRAS, 379, 209
Sereno M., 2007, MNRAS, 380, 1207
Smail I. et al., 2007, ApJ, 654, L33
Treu T., Koopmans L. V., Bolton A. S., Burles S., Moustakas L. A., 2006, ApJ, 640, 662
Umetsu K., Takada M., Broadhurst T., 2007, Modern Phys. Lett. A, 22, 2099
Wilson G., Kaiser N., Luppino G. A., Cowie L. L., 2001, ApJ, 555, 572
Wright C. O., Brainerd T. G., 2002, preprint (astro-ph/0205297)
Zaroubi S., Squires G., de Gasperis G., Evrard A. E., Hoffman Y., Silk J., 2001, ApJ, 561, 600

This paper has been typeset from a TEX/LATEX file prepared by the author.